HHS Public Access

Author manuscript

Nat Commun. Author manuscript; available in PMC 2015 September 24.

Published in final edited form as:

Nat Commun. ; 6: 6570. doi:10.1038/ncomms7570.

Rational Design of a Chalcogenopyrylium-Based Surface-Enhanced Resonance Raman Scattering-Nanoprobe with Attomolar Sensitivity

Stefan Harmsen[#1], **Matthew A. Bedics**[#2], **Matthew A. Wall**[1,3], **Ruimin Huang**[1], **Michael R. Detty**[2], and **Moritz F. Kircher**[1,4,5]

[1]Department of Radiology, Memorial Sloan Kettering Cancer Center, 1275 York Avenue, New York, New York 10065, United States

[2]Department of Chemistry, University at Buffalo, The State University of New York, Buffalo, New York 14260-3000, United States

[3]Department of Chemistry, Hunter College of the City University of New York, 695 Park Avenue, New York, New York 10065, United States

[4]Center for Molecular Imaging and Nanotechnology (CMINT), Memorial Sloan-Kettering Cancer Center, 1275 York Avenue, New York, New York 10065, United States

[5]Department of Radiology, Weill Cornell Medical College, 445 East 69th Street, New York, New York 10021, United States

[#] These authors contributed equally to this work.

Abstract

High sensitivity and specificity are two desirable features in biomedical imaging. Raman imaging has surfaced as a promising optical modality that offers both. Here, we report the design and synthesis of a group of near infrared absorbing 2-thienyl-substituted chalcogenopyrylium dyes tailored to have high affinity for gold. When adsorbed onto gold nanoparticles, these dyes produce biocompatible SERRS-nanoprobes with attomolar limits of detection amenable to ultrasensitive *in vivo* multiplexed tumor and disease marker detection.

Corresponding Authors: Moritz F. Kircher, MD, PhD, Center for Molecular Imaging and Nanotechnology, Memorial Sloan Kettering Cancer Center, Mortimer B. Zuckerman Research Center, New York, NY 10065, Phone: 646-888-3371, kircherm@mskcc.org; Michael R. Detty, PhD, Chair, Chemistry Department, University at Buffalo, NSC 627, North Campus, Buffalo, NY 14260-3000, Phone: 716-645-4228, mdetty@buffalo.edu.

Author Contributions

S.H. and M.A.B. performed the experiments, analyzed the data, and wrote the paper. M.A.W. and R.H. participated in performing the experiments. M.F.K. and M.R.D. supervised the study cand advised on experimental design, analyzed data, and edited the paper.

Competing financial interests

The authors declare no competing financial interests.

Introduction

Surface-enhanced Raman scattering (SERS) is rapidly gaining interest in the field of biomedical imaging.[1, 2, 3] By adsorbing a molecule on a noble metal surface, the weak Raman scattering of a molecule (only 1 in ~10^7 photons induces Raman scattering) is massively amplified (enhancement factor $10^7 – 10^{10}$).[4, 5, 6] This phenomenon creates a spectroscopic technique that not only has high sensitivity (10^{-9} M – 10^{-12} M limits of detectability), but also the potential for multiplexing capabilities due to the unique vibrational structure of adsorbed molecules.[7, 8, 9] These characteristics have prompted the use of SERS in a wide array of biomedical imaging applications.[2, 10, 11, 12, 13, 14, 15, 16, 17] Orders-of-magnitude higher sensitivities ($10^{-12} – 10^{-14}$ M) can be achieved utilizing Raman reporters that are in resonance with the incident laser, thereby producing surface-enhanced resonance Raman scattering (SERRS) nanoprobes.[18, 19, 20] Absorption of light by biological tissue is minimal in the near-infrared (NIR) window and, as a consequence, most optical biomedical applications use NIR detection lasers. While a great deal of attention has been given to dye molecules that absorb light in the visible region, less work has been devoted to developing Raman reporters with absorption maxima that are resonant with NIR detection lasers. The most common Raman reporters are members of the cyanine class of dyes.[21]

Herein we report thiophene-substituted chalcogenopyrylium (CP) dyes as a new class of ultra bright, NIR-absorbing Raman reporters. One notable feature of the pyrylium dyes is the ease in which a broad range of absorptivities can be accessed, and consequently be matched with the NIR light source by careful tuning of the dye's optical properties. Specifically, the large differences in absorption maxima introduced by switching the chalcogen atom is a useful property of this dye class.[22] Another important consideration is the affinity of the reporter for the surface of gold. Since the SERS effect decreases exponentially as a function of distance from the nanoparticle,[23] it is important that the Raman reporter is near the gold surface. The 2-thienyl substituent provides a novel attachment point to gold for Raman reporters. The 2-thienyl group is not only part of the dye chromophore, but also can be rigorously coplanar with the rest of the chromophore.[24] This allows the dye molecules to be in close proximity to the nanoparticle surface, creating a brighter SERRS-signal.

Results

Chalcogenopyrylium dye synthesis and characterization

Cationic chalcogenopyrylium dyes **1**–**3**, with absorption maxima near the 785-nm emission of the detection laser were synthesized as outlined in Figure 1A. The addition of MeMgBr to the known chalcogenopyranones[25] (**4**, **6**), followed by dehydration with the appropriate acid (HZ), yields 4-methyl pyrylium compounds (**5**, **7**) with the desired counterion (PF_6^- or ClO_4^-)[22, 26, 27] The condensation of **7** with *N*,*N*-dimethylthioformamide in Ac_2O, and subsequent hydrolysis of the intermediate iminium salt yields the (chalcogenopyranylidene)acetaldehyde **8**, the penultimate compound leading to trimethine chalcogenopyrylium dyes.[22] Condensation of 4-methylpyrylium salt **5** and the (chalcogenopyranylidene)acetaldehyde **8** bearing the desired R groups and chalcogen atom in hot Ac_2O[26] forms the final dye compounds **1**–**3** that are substituted with 2-phenyl or 2-thienyl groups, and different combinations of chalcogen atoms (S or Se) (Table 1). The Cl^-

and Br^- counterions of dye **1a** were accessed by treating the PF_6^- salts with an Amberlite® ion exchange resin.

SERRS-nanoprobe synthesis and characterization

Chalcogenopyrylium dyes **1**–**3** were dissolved in dry *N*,*N*-dimethylformamide (DMF), at a concentration between 1.0 and 10 mM, and were subsequently used to generate the SERRS-nanoprobes. The SERRS-nanoprobes consist of a gold core onto which the SERRS-reporter is adsorbed, which is then protected by an encapsulating silica layer (Figure 1B, Table 1). The pyrylium based SERRS-nanoprobes were synthesized by encapsulating 60 nm spherical citrate-capped gold nanoparticles via a modified Stöber procedure[28, 29, 30] in the presence of the reporter. After 25 minutes, the reaction was quenched by the addition of ethanol and the SERRS-nanoprobes were collected through centrifugation. Typically, the as-synthesized SERRS-nanoprobes had a mean diameter of ~100 nm (non-aggregated; Supplementary Figure 1 and 2).

Effect of counterion on colloidal stability and SERRS-signal

In previous reports, the dye counterion was shown to affect the structural and electronic properties of polymethine dyes[31] and the solubility of chalcogenopyrylium dyes.[32] Since SERRS is highly dependent on these factors, we evaluated the effect of the counterion (Z^-) on the SERRS spectrum, intensity, and colloidal stability of the pyrylium-based SERRS-nanoprobes. We compared chloride (Cl^-), bromide (Br^-), perchlorate (ClO_4^-), and hexafluorophosphate (PF_6^-) as counterions for chalcogenopyrylium dye **1a**. The SERRS-nanoprobes were synthesized in the presence of equimolar amounts (10 μM) of CP dye **1a** Z^- **(**where $Z^- = Cl^-$, Br^-, ClO_4^-, or PF_6^-). The counterion introduces almost no difference in optical properties (*e.g.* absorption maxima, extinction coefficient). Furthermore, with the exception of the chloride counter-ion, the Raman shifts and intensity of **1a** were minimally affected by the different counterions (Figure 2B). The colloidal stability, however, was shown to be highly counterion dependent (Figure 2B, Supplementary Figure 1 and Supplementary Table 1). The least chaotropic counterion, Cl^-, strongly destabilized the gold colloids and caused aggregation for SERRS-nanoprobes utilizing **1a** as a reporter as evidenced by the strong absorption between 700–900 nm. The strongest chaotropic anion, PF_6^-, did not affect colloidal stability during the synthesis of SERRS-nanoprobes as evidenced by the strong absorption at 540 nm and low absorbance between 700 – 900 nm (monomeric 60 nm spherical gold nanoparticles have an absorption maximum around 540 nm). Since the PF_6^- anion induced the least nanoparticle aggregation, it was used for further SERRS experiments.

Effect of increased affinity on colloidal stability and SERRS-signal

We also examined the SERRS-signal intensity as a function of the number of sulfur atoms in the dye. Sulfur-containing functionality has been used frequently to adhere molecules to gold,[33] with several reports using thiol or lipoic acid functional groups to add sulfur-containing functionality.[21, 34] In our structures, 2-thienyl groups attached to the 2- and 6-positions of the dye were used to bind the dyes to the gold surface. We also explored the impact of the chalcogen atoms in the chalcogenopyrylium core, switching a Se (**1a** and **2a**)

to S (**1b** and **2b**). The chalcogen switch was used to increase semi-covalent interactions with the gold surface, and also to create a chromophore that had a more resonant absorption with the 785-nm detection laser (Table 1). Chalcogenopyrylium dyes **1**–**3** were used at a final concentration of 1.0 μM, which prevented nanoparticle aggregation for dye **3**. Figure 3A shows the molecular structures of the chalcogenopyrylium dyes. The SERRS intensity of the different as-synthesized pyrylium-based SERRS-nanoprobes, which were synthesized at equimolar reporter concentrations, were measured at equimolar SERRS-nanoprobe concentrations at low laser power to prevent CCD-saturation (50 μW, 1.0 s acquisition time, 5× objective). We specifically focused on the 1600 cm^{-1} peak, which corresponds to aromatic ring stretching modes; and is a mode shared by chalcogenopyrylium dyes **1**–**3**. The SERRS-signal intensity of the 1600 cm^{-1} peak increased significantly as the number of 2-thienyl substituents increased (Figure 3B, Supplementary Table 1) without causing significant aggregation (Figure 3C, Supplementary Figure 2 and Supplementary Table 1). Thus, **3** produced the highest SERRS-signal, which was significantly more intense than **2a**/**2b** or **1a**/**1b** ($P<0.05$) and **2a**/**2b** were significantly more intense than **1a**/**1b** ($P<0.05$). There was a less noticeable, but significant, increase from the chalcogen switch in the core (**1a**/**1b** and **2a**/**2b** being significantly different ($P<0.05$)). This strongly supports the hypothesis that 2-thienyl groups are an effective means of adhering dyes to gold, resulting in brighter SERRS-nanoprobes.

Comparison of CP-dye 3 with a cyanine-based SERRS-reporter

In order to assess the quality of our optimized nanoprobe, thiopyrylium dye **3** and commercially available **IR792** (Figure 4A), which has been previously used to generate surface-enhanced resonance Raman scattering nanoprobes,[35] were studied. A direct comparison of the nanoprobes synthesized in the presence of equimolar (1.0 μM) amounts of **3** and **IR792** shows a 5–6-fold higher signal for nanoprobes generated with dye **3** (Figure 4B). It is interesting to note that a fluorescence background is minimal in the SERRS spectra of the CP- and cyanine-based SERRS-nanoprobes (Supplementary Figure 3). Whereas fluorescence interference would not be expected from chalcogenopyrylium dyes containing heavy chalcogens that enhance intersystem crossing,[36] fluorescence interference could be expected for the cyanine dye **IR792**. In fact, when equimolar amounts of the CP dyes **1**–**3** and **IR792** were incorporated in silica (without gold nanoparticle), **IR792** demonstrated strong fluorescence when excited at 785 nm (50 μW, 1.0 s acquisition time), while minimal fluorescence was observed for CP **1**–**3**. As shown in Figure 4B and Supplementary Figure 3, the fluorescence interference of the cyanine dye **IR792** is minimal in its SERRS spectrum. This is due to quenching effects near the surface of the nanoparticle.[37]

A concentration series of the as-synthesized SERRS-nanoprobes was generated in triplicate fashion (Supplementary Figure 4) to determine the limit of detection (LOD) of both nanoprobes. Figure 4C shows the LOD for **IR792** based nanoprobes to be 1.0 fM, while **3**-based nanoprobes had a 10-fold lower LOD, 100 aM. To our knowledge this is the lowest reported LOD utilizing a biologically relevant NIR excitation source. We also evaluated the serum stability of the **3**-based SERRS-nanoprobe. The SERRS-nanoprobe was shown to be serum stable (e.g. no significant difference between t = 1 h and t = 48 h) for at least 48 hours (Supplementary Figure 5; Supplementary Methods). This is supported by a study by Thakor

et al. who have shown that SERS-nanoparticles of similar size and composition remain stable *in vivo* for more than 2 weeks.[38]

In vivo comparison of EGFR-targeted CP3- or IR792-SERRS-nanoprobes

The ability of our SERRS-nanoprobe to delineate tumor tissue *in vivo* was assessed by utilizing CP dye **3** and **IR792**-based SERRS-nanoprobes functionalized with an epidermal growth factor receptor (EGFR)-targeting antibody. Equimolar amounts (15 fmol/g) of these two EGFR-targeted nanoprobes were injected intravenously into athymic nude mice which had been inoculated two weeks prior with the EGFR-overexpressing cell line A431 (1×10^6 cells). After 18 hours, the skin around the tumor was carefully peeled back and multiplexed Raman imaging the tumor site and surrounding tissue was performed (Figure 5–6). A Raman map was generated and the signals from the multiplexed SERRS-nanoprobes were deconvoluted by applying a direct classical least square algorithm (DCLS).[7] The SERRS-signal from both nanoprobes was more intense for the tumor site than for the surrounding tissue, showing that the EGFR-targeted SERRS-nanoprobes had selectively localized at the tumor site. The SERRS-signal intensity at the tumor mass revealed a 3× higher signal density for the **3**-based SERRS-nanoprobes than for the otherwise identical **IR792**-based SERRS-nanoprobes. *Ex vivo* multiplexed Raman imaging of the tumor showed Raman signal of the EGFR-targeted SERRS-nanoprobes throughout the tumor with the exception of a hypointense Raman region in the center of the tumor. H&E and immunohistochemical staining for EGFR was performed (Supplementary Methods) and revealed that the hypointense Raman region corresponded with an area of necrosis, which explains the lack of SERRS-nanoprobe accumulation and decreased Raman signal. In addition, to validate EGFR targeting, we injected A431-tumor bearing mice with cetuximab (50 pmol/g) 3 hours prior to injection with the EGFR-targeted SERRS-nanoprobes. Pre-blocking of EGFR by cetuximab resulted in decreased accumulation of the EGFR-targeted SERRS-nanoprobes within the tumors of animals that were injected with cetuximab prior to EGFR-targeted SERRS-nanoprobe injection as compared to animals that were injected with EGFR-targeted SERRS-nanoprobes and were not pre-injected with cetuximab (Supplementary Figure 6).

Discussion

Effective biomedical imaging requires low limits of detection and high specificity for biological targets. Raman imaging has surfaced as an optical imaging modality that has the promise to enable both. While the Raman effect is relatively weak (1 in 10^7 photons),[3-5] the Raman scattering cross section of a molecule can be massively amplified by noble metal surfaces. Here, we demonstrated that rational SERRS-reporter design afforded SERRS-nanoprobes with unprecedented limits of detection: 100 attomolar. This is to the best of our knowledge the lowest reported limit of detection at near-real-time detection (≤2.0 s acquisition times) for SERRS-nanoprobes that are compatible with a NIR light source. As a comparison non-resonant SERS-nanoprobes are in the 0.1–1.0 pM range (1,000–10,000-fold less sensitive)[2], while reported detection limits of SERRS-nanoprobes are >17 fM at near real-time detection.[39] Others have reported a 0.4 fM detection limit, however, this was acquired through cumulative data acquisition with an acquisition time ≥60s, which is not practical for biomedical imaging applications.[35]

We believe the unprecedented limit of detection of our novel SERRS-nanoprobe is due to several factors. First, we demonstrate that rational design and optimization of the SERRS-reporter is important to achieve efficient “loading” on the nanoparticle. Our results demonstrate that the counterion and gold surface affinity are important considerations. For instance, while the chaotropic PF_6^- anions stabilized the dye-nanoparticle system during silica shell formation in ethanol, the system becomes more destabilized with Cl^- (more kosmotropic) ions present. Chloride-induced aggregation of colloidal dispersions in relation to SERS has been studied. Natan *et al.* demonstrated that the strongest enhancements were obtained from aggregates with effective diameters of less than 200nm and aggregates with sizes >200nm did not generate appreciable SERS intensities.[40] The aggregates that were induced by the chloride counterion in our system were >200 nm (Supplementary Figure 2), which might explain the reduced SERRS-signal when chloride is used as a counterion. Others have shown that the kosmotropic chloride-ion could induce reorientation of the dye on the surface, which could also contribute to the reduced SERRS intensities.[41] However, while we did observe a decrease in the SERRS-signal intensity when chloride is present, we did not find any appreciable differences between the Raman spectra of the dyes when different counterions were use, which would have been expected if the molecule had reoriented on the surface. Since the most chaotropic counterion, PF_6^-, induced the least aggregation and generated robust SERRS-signal intensities, we used PF_6^- as a counterion.

Next, we showed that an increase in affinity of the SERRS-reporter for the gold nanoparticle surface via incorporation of 2-thienyl functional groups considerably increased the SERRS-signal without inducing aggregation. Others have reported the functionalization of NIR dyes with thiol or lipoic acid functional groups. In contrast to a 2-thienyl substituent, thiol and lipoic acid functional groups offer no benefit to the optical properties of the dye, and as a tether, do not allow the dye to be as close to the gold surface. Moreover, based on the absorption spectra of reported lipoic-acid modified cyanine dye-gold nanoparticle conjugates, it is clear that lipoic-acid modified dyes promote aggregation.[21, 34]

Finally, the strategy chosen to stabilize the SERRS-nanoprobe is a key factor. Others have reported using either surfactants or thiolated-polymers to stabilize their SERRS-nanoparticles.[35, 39, 42] However, such stabilizing agents compete with the SERRS-reporter for the surface of the nanoparticle, which leads to relatively low SE(R)RS-signal. We achieved very low limits of detection by using a primerless silication procedure in which the silica not only served as a stabilizing agent, but also as a matrix to contain our optimized CP-based SERRS-reporter. Since silica has much lower affinity for the gold than the applied SERRS-reporters, attomolar limits of detection were achieved.

The chalcogenopyrylium dyes represent a new class of SERRS-reporters. Selection of the right combination of chaotropic counterions and increased affinity of the SERRS-reporter for the gold nanoparticle’s surface produces stable SERRS-nanoprobes with exceptionally low limits of detection (attomolar range). The low limit of detection (*i.e.* close to single nanoparticle detection) in combination with the high resolution of Raman imaging, enables highly sensitive and specific, near-real-time tumor delineation and, as a result of the fingerprint like spectra of the different SERRS-nanoprobes, can offer multiplexed disease marker detection *in vivo*.

Methods

Materials

Acetonitrile (99.9%), sodium borohydride (98%) and sodium bicarbonate (99%) were used as received from Fisher Scientific (Pittsburg, PA). Methyl magnesium bromide (3.0 M in tetrahydrofuran), hexafluorophosphoric acid (60% (w/v)), perchloric acid (60% (w/v)), Amberlite® IRA-400(Cl) ion exchange resin, *N*,*N*-dimethylthioformamide (98%), potassium hydroxide (85%), acetic anhydride (99.7%), gold chloride trihydrate (99.9%), ammonium hydroxide (28% (v/v) 99.99% purity), tetraethyl orthosilicate (TEOS; 99.999%), mercaptotrimethoxysilane (MPTMS), ethanol (anhydrous, 99.5%), 2-(*N*-morpholino)ethanesulfonic acid (MES), IR792 perchlorate, heterobifunctional polyethylene glycol (4000 Da; maleimide/N-hydroxysuccinimide(NHS)) were used as received from Sigma Aldrich (St.Louis, MO.). Cetuximab (2mg/ml; Genentech, South San Francisco, CA) was provided by the Memorial Sloan Kettering Cancer Center Hospital Pharmacy. All chromatographic separations were performed on silica gel (SiO_2; 60 Å, Scientific Absorbents Inc.). Tetrahydrofuran (THF) was distilled from a sodium benzophenone ketyl still prior to use.

Chalcogenopyrylium dye synthesis and characterization

All reactions were done open to air unless otherwise noted. Concentration *in vacuo* was performed on a rotary evaporator. NMR spectra were recorded at 300 or 500 MHz for ^1H and at 75.5 MHz for ^{13}C with residual solvent signal as internal standard. If a mixture of CD_2Cl_2 and CD_3OD was used to acquire ^1H NMR, the peak for CH_2Cl_2 was used as the internal standard. UV/VIS-near-IR spectra were recorded in quartz cuvettes with a 1-cm path length. Melting points were determined with a capillary melting point apparatus and are uncorrected. Non-hygroscopic compounds have a purity of ≥ 95% as determined by elemental analyses for C, H, and N. Experimental values of C, H, and N are within 0.3% of theoretical values. ^{13}C NMR was not recorded for pyrylium dyes due to limited solubility in common NMR solvents. Chalcogenopyranones[25] **4** and **6** were made according to literature procedures as were 4-methylchalcogenopyrylium and 4-methylchalcogenobenzopyrylium compounds **5** and **7**.[22, 25, 26, 27]

Preparation of 4-(2,6-di(thiophen-2-yl)-4H-thiopyran-4ylidene)acetaldehyde (8, Y=S, R_2=2-thienyl)—4-Methyl-2,6-di(thiophen-2-yl)thiopyrylium hexafluorophosphate (0.350 g, 0.833 mmol), *N*,*N*-dimethylthioformamide (0.213 mL, 2.50 mmol) and Ac_2O (3.0 mL) were combined in a small round bottom flask and heated at 95 °C for 1 h. After cooling to ambient temperature an additional portion of Ac_2O (2.0 mL) was added and the solution diluted with ether. The formed iminium salt was allowed to precipitate in the freezer over night, and then isolated by filtration to yield a bright orange solid. This solid was dissolved in CH_3CN (3.0 mL) and satd. aqueous $NaHCO_3$ (3.0 mL) was added. This mixture was heated to 80 °C over 15 min, and kept at that temperature for 30 min. After diluting with H_2O (30 mL) the product was extracted with CH_2Cl_2 (3 × 50 mL), dried with Na_2SO_4 and purified on SiO_2 with a 10% EtOAc/CH_2Cl_2 eluent (R_f = 0.71) to yield a yellow oil that was recrystallized in CH_2Cl_2/hexanes to yield 0.219 g (87%) of a yellow crystalline solid, mp 143-144 °C: ^1H NMR [500 MHz, $CDCl_3$] 9.84 (d, 1 H, *J* = 6.0 Hz), 8.26 (s, 1 H), 7.45-7.39

(m, 4 H), 7.13-7.11 (m, 2 H), 6.88 (s, 1 H), 5.72 (d, 1 H, *J* = 6.5 Hz); ^{13}C NMR [75.5 MHz, $CDCl_3$] δ 188.05, 146.43, 139.36, 139.07, 137.33, 136.65, 128.16, 127.78, 127.58, 126.30, 126.01, 122.48, 117.63, 117.48; HRMS (ESI) *m/z* 302.9971 (calcd for $C_{15}H_{11}O_1S_3$: 302.9967).

Preparation of 4-(2,6-diphenyl-4H-selenopyran-4ylidene)acetaldehyde (8, Y=Se, R_2=Ph)—4-methyl-2,6-di(phenyl)selenopyrylium hexafluorophosphate (0.200 g, 0.439 mmol), *N*,*N*-dimethylthioformamide (0.112 mL, 1.32 mmol) and Ac_2O (4.0 mL) were added to a round-bottom flask and heated at 95 °C for 90 min. After cooling to rt CH_3CN (4.0 mL) was added and the product precipitated by addition of ether and chilling overnight in the freezer. The iminium salt was isolated by filtration, and hydrolyzed by dissolving in CH_3CN (4.0 mL), adding satd. aqueous $NaHCO_3$ (4.0 mL) and heating the mixture to 80 °C over a 15 min period. The reaction was maintained at this temperature for 30 min, after which the reaction was diluted with H_2O (50 mL), the product extracted with CH_2Cl_2 (3 × 30 mL), dried with $MgSO_4$, and after concentration purified on SiO_2 with first a CH_2Cl_2 and then a 10% EtOAc/CH_2Cl_2 (R_f = 0.70) eluent to yield 0.122 g (82%) of a orange oil: ^{1}H NMR [500 MHz, $CDCl_3$] δ 10.11 (d, 1 H, *J* = 10.5 Hz), 8.32 (s, 1 H), 7.62-7.46 (m, 9 H), 7.00 (s, 1 H), 5.88 (d, 1 H, *J* = 11.0 Hz); ^{13}C NMR [75.5 MHz, $CDCl_3$] δ 188.69, 148.44, 147.01, 146.03, 138.65, 138.40, 129.96, 129.90, 129.14, 126.62, 126.44, 126.37, 126.31, 125.67, 120.57, 120.48; HRMS (EI) *m/z* 339.0292 (calcd for $C_{19}H_{15}O^{80}Se$: 339.0283).

Preparation of 4-(3-(2,6-diphenyl-4H-selenopyran-4-ylidene)prop-1-enyl)-2,6-diphenylselenopyrylium (1a) (CAS Registry Number: 51848-65-8)

PF_6^-: 4-methyl-2,6-di(phenyl)selenopyrylium hexafluorophosphate (0.190 g, 0.417 mmol), 4-(2,6-diphenyl-4H-selenopyran-4ylidene)acetaldehyde (0.155 g, 0.459 mmol) and Ac_2O (3.0 mL) were combined in a round bottom flask and heated at 105 °C for 10 min. The reaction was cooled to ambient temperature, precipitated with ether, and the collected solid recrystallized from CH_3CN/ether to yield 0.278 g (86%) of a golden-green solid: ^{1}H NMR [500 MHz, CD_2Cl_2] δ 8.59 (t, 1 H, *J* = 13.5 Hz), 8.40-7.80 (br s, 4 H), 7.71 (d, 8 H, *J* = 7.0 Hz), 7.63-7.59 (m, 12 H), 6.85 (d, 2 H, *J* = 13.0 Hz); Anal. Calcd for $C_{37}H_{27}Se_2$ PF_6: C, 57.38; H, 3.51; F, 14.72. Found: C, 57.34; H, 3.48; F, 14.76; LRMS (ESI) *m/z* 631.2 (calcd for $C_{37}H_{27}{}^{80}Se_2$: 631.0); λ_{max} (CH_2Cl_2) = 806 nm, ε = 2.5 × 10^5 $M^{-1}cm^{-1}$.

ClO_4^-: 4-methyl-2,6-di(phenyl)selenopyrylium perchlorate (50.0 mg, 0.122 mol), 4-(2,6-diphenyl-4H-selenopyran-4ylidene)acetaldehyde (81.4 mg, 0.241 mmol) and Ac_2O (2.0 mL) were treated as described for the PF_6 salt to yield 82.0 mg (90%) of a golden-green solid: ^{1}H NMR [500 MHz, 1:1 CD_2Cl_2:CD_3OD] δ 8.77 (t, 1 H, *J* = 13.5 Hz), 8.60-7.80 (m, 4 H), 7.71 (d, 8 H, *J* = 7.0 Hz), 7.66-7.54 (m, 12 H), 6.83 (d, 2 H, *J* = 14.0 Hz); Anal. Calcd for $C_{37}H_{27}Se_2$ ClO_4: C, 60.96; H, 3.73. Found: C, 60.69; H, 3.83; λ_{max} (CH_2Cl_2) = 806 nm, ε = 2.5 × 10^5 $M^{-1}cm^{-1}$.

Cl^-: The hexafluorophosphate salt (50 mg) was converted to the chloride salt by treating with Amberlite® IRA-400 chloride form (200 mg) in a 1:1 CH_2Cl_2:MeOH mixture (3.0 mL). This process was repeated two more times after which the product was dissolved in CH_2Cl_2, washed with water, the organic layer dried with Na_2SO_4, filtered over Celite®, and

after concentration recrystallized from CH_3CN/ether to yield a bronze solid: ^{1}H NMR [500 MHz, 3:1 CD_3OD:CD_2Cl_2] δ 8.87 (t, 1 H, *J* = 13.0 Hz), 8.40-7.80 (m, 4 H), 7.70 (d, 8 H, *J* = 7.0 Hz), 7.56-7.50 (m, 12 H), 6.84 (d, 2 H, *J* = 13.0 Hz); Anal. Calcd for $C_{37}H_{27}Se_2 \cdot Cl \cdot 4/3H_2O$: C, 64.50; H, 4.34; Cl, 5.15. Found: C, 64.54; H, 4.42; Cl, 4.98; λ_{max} (CH_2Cl_2) = 806 nm,ε = 2.3 × 10^5 $M^{-1}cm^{-1}$.

Br^-: The hexafluorophosphate salt (50 mg) was converted to the bromide salt by treating with Amberlite® IRA-400 bromide form (200 mg) in a 1:1 CH_2Cl_2:MeOH mixture (3.0 mL). This process was repeated two more times after which the product was dissolved in CH_2Cl_2, washed with water, the organic layer dried with Na_2SO_4, filtered over Celite®, and after concentration recrystallized from CH_3CN/ether to yield a bronze solid: ^{1}H NMR [500 MHz, 3:2 CD_2Cl_2:CD_3OD] δ 8.79 (t, 1 H, *J* = 13.5 Hz), 8.40-7.80 (br s, 4 H), 7.71 (d, 8 H, *J* = 7.0 Hz), 7.60-7.54 (m, 12 H), 8.50 (d, 2 H, *J* = 13.0 Hz); Anal. Calcd for $C_{37}H_{27}Se_2$ Br H_2O: C, 61.09; H, 4.02; Br, 10.98. Found: C, 61.08; H, 3.89; Br, 10.77; λ_{max} (CH_2Cl_2) = 806 nm, ε = 2.3 × 10^5 $M^{-1}cm^{-1}$.

Preparation of 4-(3-(2,6-diphenyl-4H-thiopyran-4-ylidene)prop-1-enyl)-2,6-diphenylselenopyrylium hexafluorophosphate (1b) (CAS Registry Number: 79054-92-5)—4-Methyl-2,6-di(phenyl)thiopyrylium hexafluorophosphate (0.128 g, 0.312 mmol), 4-(2,6-diphenyl-4H-selenopyran-4ylidene)acetaldehyde (0.157 g, 0.344 mmol) and Ac_2O (2.0 mL) were combined in a round bottom flask and heated at 105 °C for 10 min. The reaction was cooled to ambient temperature, CH_3CN (2.0 mL) was added and ether was used to precipitate product from solution to yield 0.196 g (86%) of a copper-bronze solid: ^{1}H NMR [500 MHz, CD_2Cl_2] δ 8.54 (t, 1 H, *J* = 13.0 Hz), 8.20-7.80 (br s, 4 H), 7.78 (d, 4 H, *J* = 8.0 Hz), 7.70 (d, 4 H, *J* = 7.5 Hz), 7.66-7.58 (m, 12 H), 6.78 (d, 2 H, *J* = 13.5 Hz); Anal. Calcd for $C_{39}H_{34}O_3Se_2$ PF_6: C, 61.08; H, 3.74. Found: C, 61.10; H, 3.68; LRMS (ESI) *m/z* 583.3 (calcd for $C_{37}H_{27}S^{80}Se$: 583.1); λ_{max} (CH_2Cl_2) = 784 nm, ε = 2.0 × 10^5 $M^{-1}cm^{-1}$.

Preparation of 4-(3-(2,6-dithiophen-2-yl-4H-thiopyran-4-ylidene)prop-1-enyl)-2,6-diphenylselenopyrylium (2a)—4-methyl-2,6-di(phenyl)selenopyrylium hexafluorophosphate (0.102 g, 0.225 mmol), 4-(2,6-(thiophen-2-yl)-4H-thiopyran-4ylidene)acetaldehyde (75.0 mg, 0.248 mmol) and Ac_2O (3.0 mL) were combined in a round bottom flask and heated at 105 °C for 5 min. The reaction was cooled to ambient temperature, precipitated with ether, and the collected solid recrystallized from CH_3CN/ether to yield 0.145 g (87%) of a bronze solid, mp 229-231 °C: ^{1}H NMR [500 MHz, CD_2Cl_2] δ 8.46 (t, 1 H, *J* = 13.0 Hz), 7.71-7.58 (m, 18 H), 7.26 (t, 2 H, *J* = 4.0 Hz), 6.77 (d, 1 H, *J* = 13.0 Hz), 6.70 (d, 1 H, *J* = 14.0 Hz); Anal. Calcd for $C_{33}H_{23}S_3Se$ PF_6: C, 53.59; H, 3.13; F, 15.41. Found: C, 53.79; H, 3.13; F, 15.19; HRMS (ESI) *m/z* 595.0125(calcd for $C_{33}H_{23}S_3{}^{80}Se$: 595.0122); λ_{max} (CH_2Cl_2) = 810 nm, ε = 2.5 × 10^5 $M^{-1}cm^{-1}$.

Preparation of 4-(3-(2,6-dithiophen-2-yl-4H-thiopyran-4-ylidene)prop-1-enyl)-2,6-diphenylthiopyrylium hexafluorophosphate (2b)—4-Methyl-2,6-diphenylthiopyrylium hexafluorophosphate (30.0 mg, 73.0 μmol), 4-(2,6-(thiophen-2-yl)-4H-thiopyran-4ylidene)acetaldehyde (24.4 mg, 81.0 μmol) and Ac_2O (1.0 mL) were

combined in a round bottom flask and heated at 105 °C for 5 min. The reaction was cooled to ambient temperature, CH_3CN (4.0 mL) was added and ether was used to precipitate product from solution to yield 45.0 mg (88%) of a bronze solid, mp > 260 °C: ^{1}H NMR [500 MHz, CD_2Cl_2] δ 8.44 (t, 1 H, *J* = 13.0 Hz), 8.40-7.80 (br s, 4 H), 7.78 (d, 4 H, *J* = 7.0 Hz), 7.67-7.59 (m, 10 H), 7.24 (t, 2 H, *J* = 4.5 Hz), 6.71 (d, 1 H, *J* = 13.0 Hz), 6.63 (d, 1 H, *J* = 13.5 Hz); Anal. Calcd for $C_{33}H_{23}S_4$ PF_6: C, 57.21; H, 3.35. Found: C, 56.97; H, 3.36; HRMS (ESI) *m/z* 547.0674 (calcd for $C_{33}H_{23}S_4$: 547.0677); λ_{max} (CH_2Cl_2) = 789 nm, ε = 2.2×10^5 M^{-1} cm^{-1}.

Preparation of 4-(3-(2,6-dithiophen-2-yl-4H-thiopyran-4-ylidene)prop-1-enyl)-(2,6-dithiophen-2-yl)thiopyrylium hexafluorophosphate (3) (CAS Registry Number: 95410-36-9)—4-Methyl-2,6-di(thiophen-2-yl)thiopyrylium hexafluorophosphate (11.0 mg, 26.2 μmol), 4-(2,6-(thiophen-2-yl)-4H-thiopyran-4ylidene)acetaldehyde (9.5 mg, 31.4 μmol) and Ac_2O (1.0 mL) were combined in a round bottom flask and heated at 105 °C for 5 min. The reaction was cooled to ambient temperature, CH_2Cl_2 (2.0 mL) was added and ether was used to precipitate product from solution to yield 17.8 mg (94%) of a bronze solid, mp > 260 °C: ^{1}H NMR [500 MHz, CD_3CN] δ 8.32 (t, 1 H, *J* = 13.5 Hz), 7.68 (d, 2 H, *J* = 4 Hz), 7.56 (br. s, 4 H) 7.14 (t, 4 H, *J* = 4.5 Hz), 6.48 (d, 2 H, *J* = 13.0 Hz); Anal. Calcd for $C_{29}H_{19}S_6$ PF_6: C, 49.42; H, 2.72. Found: C, 49.19; H, 2.79; HRMS (ESI) *m/z* 558.9805 (calcd for $C_{29}H_{19}S_6$: 558.9806); λ_{max} (CH_2Cl_2) = 813 nm, ε = 2.8×10^5 $M^{-1}cm^{-1}$. Spectral data agree with published spectra.[43]

SERRS-nanoprobe synthesis

Gold nanoparticles were synthesized through addition of 7.5 mL 1% (w/v) sodium citrate to 1.0 L boiling 0.25 mM $HAuCl_4$. The as-synthesized gold nanoparticles were concentrated by centrifugation (10 min, 7500 × *g*, 4 °C) and dialyzed overnight (3.5 kDa MWCO; 5 L 18.2 MΩ·cm). The dialyzed gold nanoparticles (100 μL; 2.0 nM) were added to 1000 μL absolute ethanol in the presence of 30 μL 99.999% tetraethyl orthosilicate (Sigma Aldrich), 15 μL 28% (v/v) ammonium hydroxide (Sigma Aldrich) and 1 μL chalcogenopyrylium dye (1–10 mM) in *N*,*N*-dimethylformamide. After shaking (375 rpm) for 25 min at ambient conditions in a plastic container, the SERRS-nanoprobes were collected by centrifugation, washed with ethanol, and redispersed in water to yield 2.0 nM SERRS-nanoprobes.

SERRS-nanoprobe characterization

The as-synthesized SERRS-nanoprobes were characterized by transmission electron microscopy (TEM; JEOL 1200ex-II, 80 kV, 150,000× magnification) to study the SERRS-nanoprobe structural morphology. The size and concentration of the SERRS-nanoprobes were determined on a Nanoparticle Tracking Analyzer (NTA; Malvern Instruments, Malvern, UK). Absorption spectra to determine possible nanoparticle aggregation (typically detectable at wavelengths > 600 nm) were measured on an M1000Pro spectrophotometer (Tecan Systems Inc. San Jose, CA). Finally Raman spectra were acquired on a Renishaw InVIA system equipped with a 785-nm laser (Renishaw Inc, Hoffman Estates, IL). All measurements were performed at a laser power of 50 μW (1.0 s acquisition time, 5× objective).

SERRS-nanoprobe limit of detection

SERRS-nanoprobes were synthesized as described above in the presence of an equimolar (1.0 μM) amount of **3** or **IR792**. SERRS imaging to determine the limit of detection was performed at 100 mW (2.0 s acquisition time (StreamLime™), 5× objective) on a phantom that consisted of a serial diluted **IR792**- or chalcogenopyrylium dye **3**-based SERRS-nanoprobe redispersed in 10 μL water (concentration range 3000 – 0.003 fM; n=3). The Raman maps were generated by WiRE 3.4 software (Renishaw) by applying a direct classical least square (DCLS) algorithm. The Raman image was analyzed with ImageJ software and plotted in GraphPad Prism (GraphPad Software Inc., La Jolla, CA).

Animal studies

All animal experiments were approved by the Institutional Animal Care and Use Committees of Memorial Sloan Kettering Cancer Center.

In vivo comparison of EGFR-targeted CP3- or IR792-SERRS-nanoprobes

Eight-to-ten week-old female athymic nude mice (n=5; Hsd:Athymic Nude-*Foxn1*^{nu}; Harlan Laboratories) were subcutaneously inoculated with the EGFR-overexpressing cell line A431 (1×10^6 cells; ATCC CRL-1555). After 2 weeks, the mice were injected with an equimolar amount (15 fmol/g) of EGFR-targeted **IR792**- and **3**-based SERRS-nanoprobes. The EGFR-targeted SERRS-nanoprobes were synthesized as described above in the presence of an equimolar (1.0 μM) amount of **3** or **IR792**. The as-synthesized SERRS-nanoprobes were subsequently functionalized with sulfhydryl-groups by heating the SERRS-nanoprobes in 5 mL 2% (v/v) mercaptotrimethoxysilane (MPTMS) in ethanol at 70 °C for 2 hours. The sulfhydryl-functionalized SERRS-nanoprobes were washed with water, redispersed in 10 mM MES buffer (pH 7.1), and conjugated to an EGFR-targeting antibody (cetuximab; Genentech, South San Francisco, CA) with a 4000 Da heterobifunctional maleimide/*N*-hydroxysuccinimide polyethylene glycol linker.[44] Eighteen hours later, the mice were sacrificed by CO_2-asphyxiation. The tumor was exposed and scanned by Raman imaging (10 mW, 1.5 s acquisition time (StreamLime™), 5× objective). The Raman maps were generated by WiRE 3.4 software (Renishaw) by applying a direct classical least square (DCLS) algorithm.

Supplementary Material

Refer to Web version on PubMed Central for supplementary material.

Acknowledgments

The authors would like to thank the Electron Microscopy and Molecular Cytology Core Facility at Memorial Sloan Kettering Cancer Center (MSKCC). This work was supported in part by the following grants: NIH R01 EB017748 (M.F.K.); NIH K08 CA163961 (M.F.K.); M.F.K. is a Damon Runyon-Rachleff Innovator supported (in part) by the Damon Runyon Cancer Research Foundation (DRR-29-14); MSKCC Center for Experimental Therapeutics Grant (M.F.K.). MSKCC Center for Molecular Imaging and Nanotechnology Grant (M.F.K.); MSKCC Technology Development Grant (M.F.K.); Geoffrey Beene Cancer Research Center at MSKCC Grant Award (M.F.K.) and Shared Resources Award (M.F.K.); The Dana Foundation Brain and Immuno-Imaging Grant (M.F.K.); Dana Neuroscience Scholar Award (M.F.K.); Bayer HealthCare Pharmaceuticals/RSNA Research Scholar Grant (M.F.K.); MSKCC Brain Tumor Center Grant (M.F.K.); Society of MSKCC Research Grant (M.F.K.); NIH GM-94367 (M.R.D.); and the National Science Foundation (CHE-1151379, M.R.D.). M.A.W. is supported by a National Science Foundation Integrative Graduate Education and Research Traineeship Grant (NSF, IGERT

0965983 at Hunter College). Acknowledgments are also extended to the grant-funding support provided by the NIH MSKCC Center Grant (P30 CA008748).

References

1. Wang Y, Yan B, Chen L. SERS Tags: Novel Optical Nanoprobes for Bioanalysis. Chem. Rev. 2013; 113:1391–1428. [PubMed: 23273312]
2. Kircher MF, et al. A brain tumor molecular imaging strategy using a new triple-modality MRI-photoacoustic-Raman nanoparticle. Nat. Med. 2012; 18:829–834. [PubMed: 22504484]
3. Qian X, et al. In vivo tumor targeting and spectroscopic detection with surface-enhanced Raman nanoparticle tags. Nature biotechnology. 2008; 26:83–90.
4. Kneipp K, et al. Single molecule detection using surface-enhanced Raman scattering (SERS). Phys. Rev. Lett. 1997; 78:1667–1670.
5. Nie S, Emory SR. Probing single molecules and single nanoparticles by surface-enhanced Raman scattering. Science. 1997; 275:1102–1106. [PubMed: 9027306]
6. Jeanmaire DL, Van Duyne RP. Surface Raman spectroelectrochemistry. Part I. Heterocyclic, aromatic, and aliphatic amines adsorbed on the anodized silver electrode. J. Electroanal. Chem. Interfacial Electrochem. 1977; 84:1–20.
7. Zavaleta CL, et al. Multiplexed imaging of surface enhanced Raman scattering nanotags in living mice using noninvasive Raman spectroscopy. Proc. Natl. Acad. Sci. U.S.A. 2009; 106:13511–13516. [PubMed: 19666578]
8. Faulds K, Jarvis R, Smith WE, Graham D, Goodacre R. Multiplexed detection of six labeled oligonucleotides using surface enhanced resonance Raman scattering (SERRS). Analyst. 2008; 133:1505–1512. [PubMed: 18936827]
9. Gellner M, Koempe K, Schluecker S. Multiplexing with SERS labels using mixed SAMs of Raman reporter molecules. Anal. Bioanal. Chem. 2009; 394:1839–1844. [PubMed: 19543719]
10. Craig D, McAughtrie S, Simpson J, McCraw C, Faulds K, Graham D. Confocal SERS Mapping of Glycan Expression for the Identification of Cancerous Cells. Anal. Chem. 2014; 86:4775–4782. [PubMed: 24842517]
11. Gracie K, et al. Simultaneous detection and quantification of three bacterial meningitis pathogens by SERS. Chem. Sci. 2014; 5:1030–1040.
12. McAughtrie S, Lau K, Faulds K, Graham D. 3D optical imaging of multiple SERS nanotags in cells. Chem. Sci. 2013; 4:3566–3572.
13. Sha MY, Xu H, Natan MJ, Cromer R. Surface-Enhanced Raman Scattering Tags for Rapid and Homogeneous Detection of Circulating Tumor Cells in the Presence of Human Whole Blood. J. Am. Chem. Soc. 2008; 130:17214–17215. [PubMed: 19053187]
14. Cao YC, Jin R, Mirkin CA. Nanoparticles with Raman spectroscopic fingerprints for DNA and RNA detection. Science. 2002; 297:1536–1540. [PubMed: 12202825]
15. Yuen JM, Shah NC, Walsh JT Jr. Glucksberg MR, Van Duyne RP. Transcutaneous Glucose Sensing by Surface-Enhanced Spatially Offset Raman Spectroscopy in a Rat Model. Anal. Chem. 2010; 82:8382–8385. [PubMed: 20845919]
16. McQueenie R, et al. Detection of Inflammation in Vivo by Surface-Enhanced Raman Scattering Provides Higher Sensitivity Than Conventional Fluorescence Imaging. Anal. Chem. 2012; 84:5968–5975. [PubMed: 22816780]
17. Graham D, Mallinder BJ, Whitcombe D, Smith WE. Surface enhanced resonance Raman scattering (SERRS) - a first example of its use in multiplex genotyping. Chemphyschem. 2001; 2:746–748. [PubMed: 23686925]
18. Hildebrandt P, Stockburger M. Surface-enhanced resonance Raman spectroscopy of Rhodamine 6G adsorbed on colloidal silver. J. Phys. Chem. 1984; 88:5935–5944.
19. Dieringer JA, et al. Surface-Enhanced Raman Excitation Spectroscopy of a Single Rhodamine 6G Molecule. J. Am. Chem. Soc. 2009; 131:849–854. [PubMed: 19140802]
20. Harmsen S, et al. Surface-enhanced resonance Raman scattering nanostars for high-precision cancer imaging. Sci. Transl. Med. 2015; 7:271ra277.

21. Samanta A, et al. Ultrasensitive Near-Infrared Raman Reporters for SERS-Based In Vivo Cancer Detection. Angew. Chem., Int. Ed. 2011; 50:6089–6092.
22. Detty MR, Murray BJ. Telluropyrylium dyes. 1. 2,6-Diphenyltelluropyrylium dyes. J. Org. Chem. 1982; 47:5235–5239.
23. Stiles PL, Dieringer JA, Shah NC, Van Duyne RP. Surface-enhanced Raman spectroscopy. Annu. Rev. Anal. Chem. 2008; 1:601–626.
24. Detty MR, et al. Electron Transport in 4H-1,1-Dioxo-4-(dicyanomethylidene)thiopyrans. Investigation of x-ray Structures of Neutral Molecules, Electrochemical Reduction to the Anion Radicals, and Absorption Properties and EPR Spectra of the Anion Radicals. J. Org. Chem. 1995; 60:1674–1685.
25. Leonard K, Nelen M, Raghu M, Detty MR. Chalcogenopyranones from disodium chalcogenide additions to 1,4-pentadiyn-3-ones. The role of enol ethers as intermediates. J. Heterocycl. Chem. 1999; 36:707–717.
26. Detty MR, McKelvey JM, Luss HR. Tellurapyrylium dyes. 2. The electron-donating properties of the chalcogen atoms to the chalcogenapyrylium nuclei and their radical dications, neutral radicals, and anions. Organometallics. 1988; 7:1131–1147.
27. Panda J, Virkler PR, Detty MR. A comparison of linear optical properties and redox properties in chalcogenopyrylium dyes bearing ortho-substituted aryl substituents and tert-butyl substituents. J. Org. Chem. 2003; 68:1804–1809. [PubMed: 12608794]
28. Stoeber W, Fink A, Bohn E. Controlled growth of monodisperse silica spheres in the micron size range. J. Colloid Interface Sci. 1968; 26:62–69.
29. Liz-Marzán LM, Giersig M, Mulvaney P. Synthesis of Nanosized Gold–Silica Core–Shell Particles. Langmuir. 1996; 12:4329–4335.
30. Mulvaney SP, Musick MD, Keating CD, Natan MJ. Glass-Coated, Analyte-Tagged Nanoparticles: A New Tagging System Based on Detection with Surface-Enhanced Raman Scattering. Langmuir. 2003; 19:4784–4790.
31. Bouit P-A, et al. A “Cyanine-Cyanine” Salt Exhibiting Photovoltaic Properties. Org. Lett. 2009; 11:4806–4809. [PubMed: 19795845]
32. Detty MR, Merkel PB, Hilf R, Gibson SL, Powers SK. Chalcogenapyrylium dyes as photochemotherapeutic agents. 2. Tumor uptake, mitochondrial targeting, and singlet-oxygen-induced inhibition of cytochrome c oxidase. J. Med. Chem. 1990; 33:1108–1116. [PubMed: 2157006]
33. Haekkinen H. The gold-sulfur interface at the nanoscale. Nat. Chem. 2012; 4:443–455. [PubMed: 22614378]
34. Mahajan S, Baumberg JJ, Russell AE, Bartlett PN. Reproducible SERRS from structured gold surfaces. Phys. Chem. Chem. Phys. 2007; 9:6016–6020. [PubMed: 18004415]
35. von Maltzahn G, et al. SERS-Coded Gold Nanorods as a Multifunctional Platform for Densely Multiplexed Near-Infrared Imaging and Photothermal Heating. Adv. Mater. 2009; 21:3175–3180. [PubMed: 20174478]
36. Detty MR, Merkel PB. Chalcogenapyrylium dyes as potential photochemotherapeutic agents. Solution studies of heavy atom effects on triplet yields, quantum efficiencies of singlet oxygen generation, rates of reaction with singlet oxygen, and emission quantum yields. J. Am. Chem. Soc. 1990; 112:3845–3855.
37. Dulkeith E, Ringler M, Klar TA, Feldmann J, Javier AM, Parak WJ. Gold Nanoparticles Quench Fluorescence by Phase Induced Radiative Rate Suppression. Nano Lett. 2005; 5:585–589. [PubMed: 15826091]
38. Thakor AS, et al. The fate and toxicity of Raman-active silica-gold nanoparticles in mice. Sci. Transl. Med. 2011; 3:79ra33.
39. Jokerst JV, Cole AJ, Van de Sompel D, Gambhir SS. Gold Nanorods for Ovarian Cancer Detection with Photoacoustic Imaging and Resection Guidance via Raman Imaging in Living Mice. ACS Nano. 2012; 6:10366–10377. [PubMed: 23101432]
40. Freeman RG, Bright RM, Hommer MB, Natan MJ. Size selection of colloidal gold aggregates by filtration: effect on surface-enhanced Raman scattering intensities. J. Raman Spectrosc. 1999; 30:733–738.

41. Grochala W, Kudelski A, Bukowska J. Anion-induced charge-transfer enhancement in SERS and SERRS spectra of Rhodamine 6G on a silver electrode: how important is it? J. Raman Spectrosc. 1998; 29:681.

42. Yuan H, Liu Y, Fales AM, Li YL, Liu J, Vo-Dinh T. Quantitative Surface-Enhanced Resonant Raman Scattering Multiplexing of Biocompatible Gold Nanostars for in Vitro and ex Vivo Detection. Anal. Chem. 2013; 85:208–212. [PubMed: 23194068]

43. Kudinova MA, Kurdyukov VV, Kachkovski AV, Tolmachev AI. Pyrylocyanines. 36. alpha-thienyl-substituted pyrylo- and thiopyrylocyanines. Khim Geterotsikl. 1998:494–500.

44. Chung E, et al. Use of surface-enhanced Raman scattering to quantify EGFR markers uninhibited by cetuximab antibodies. Biosensors & Bioelectronics. 2014; 60:358–365. [PubMed: 24859273]

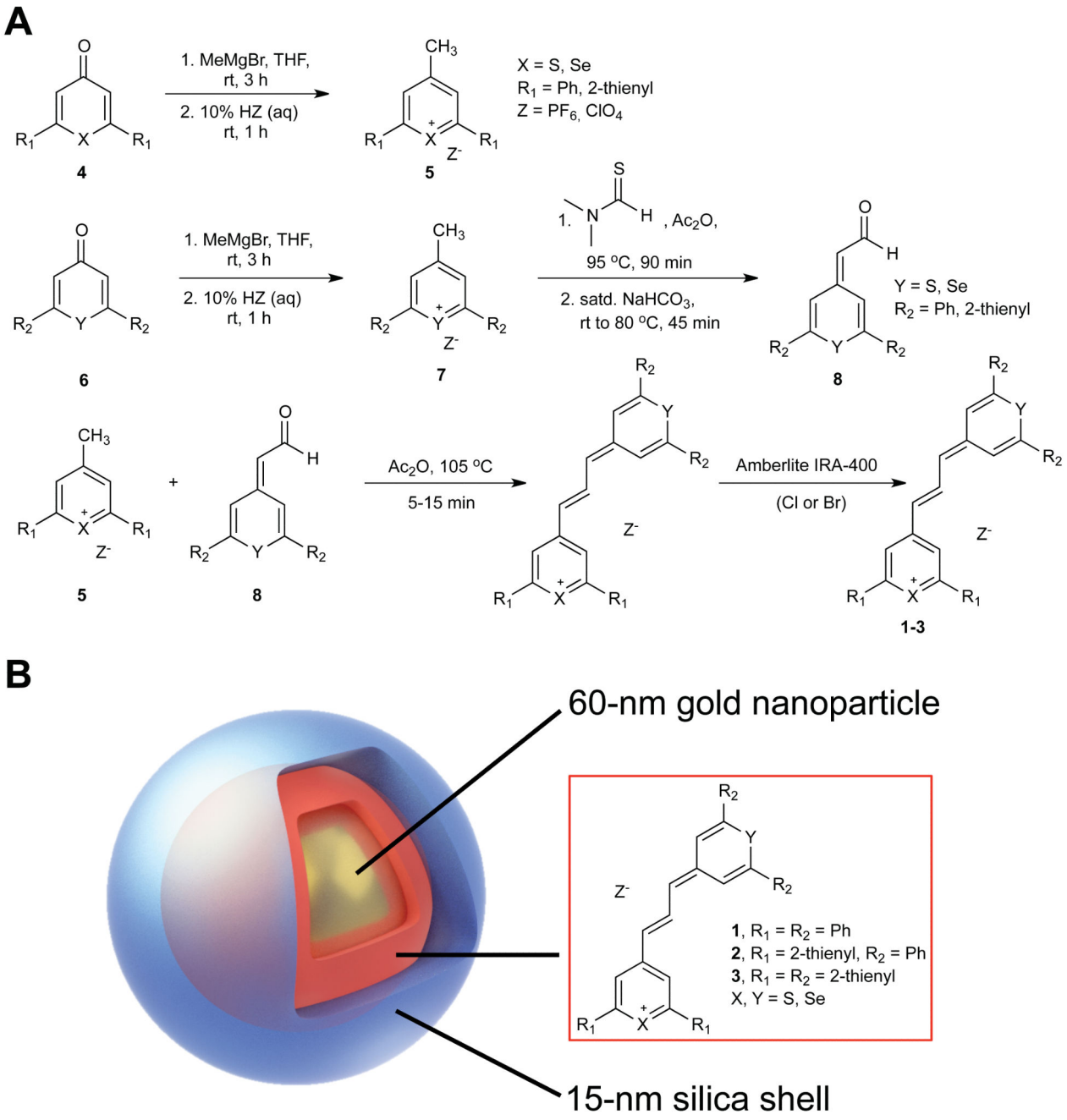

Figure 1. Synthesis and structure of the SERRS-reporters and SERRS-nanoprobe

(**A**) Reaction scheme for the synthesis of pyrylium-based SERRS-reporters (**1a**–**3**). (**B**) A 60-nm gold core (yellow) encapsulated in a 15 nm thick chalcogenopyrylium dye (red; Ph, phenyl)-containing silica shell (white). The structure, yields, and optical properties of the different chalcogenopyrylium-based Raman reporters are shown in the table.

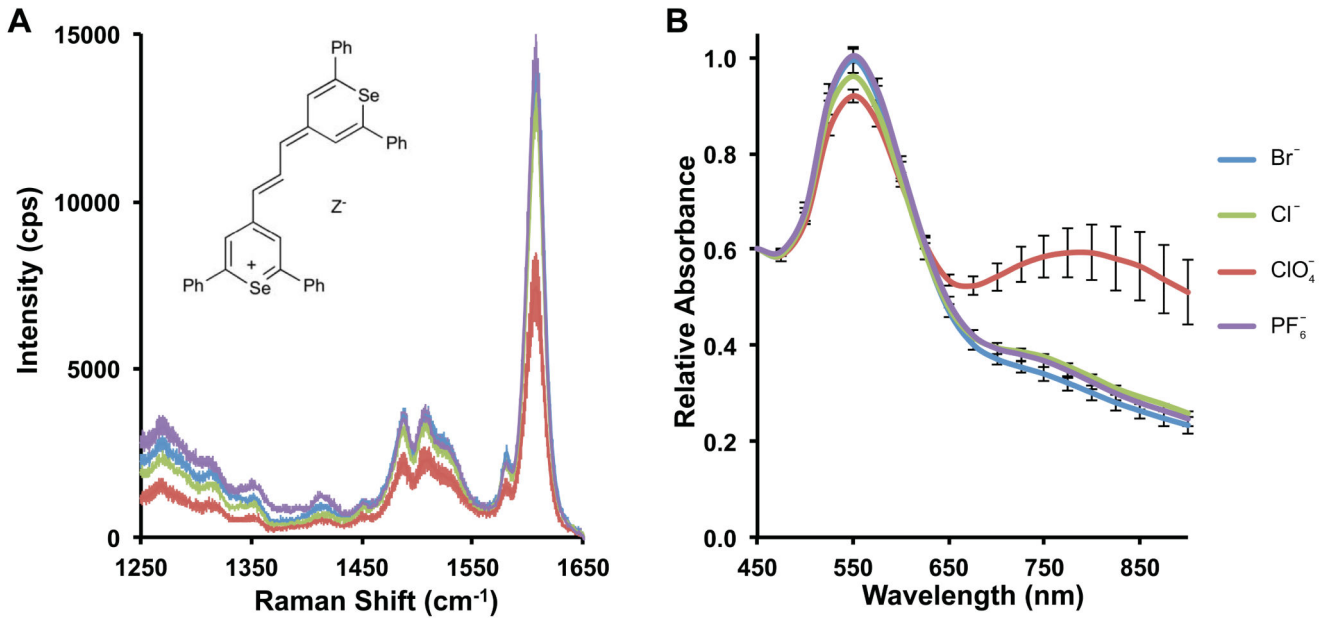

Figure 2. The effect of the counterion on colloidal stability

(**A**) The effect of the counterion (Z^-) on SERRS intensity (785 nm, 50 μW, 1.0 s acquisition time, 5× objective). Inset: Structure of CP dye **1a** (Ph, phenyl). (**B**) Effect of counterion on the colloidal stability of CP-dye **1a**-based SERRS-nanoprobes (n=3, error bars represent standard deviations; See also Supplementary Figure 1; Supplementary Table 1).

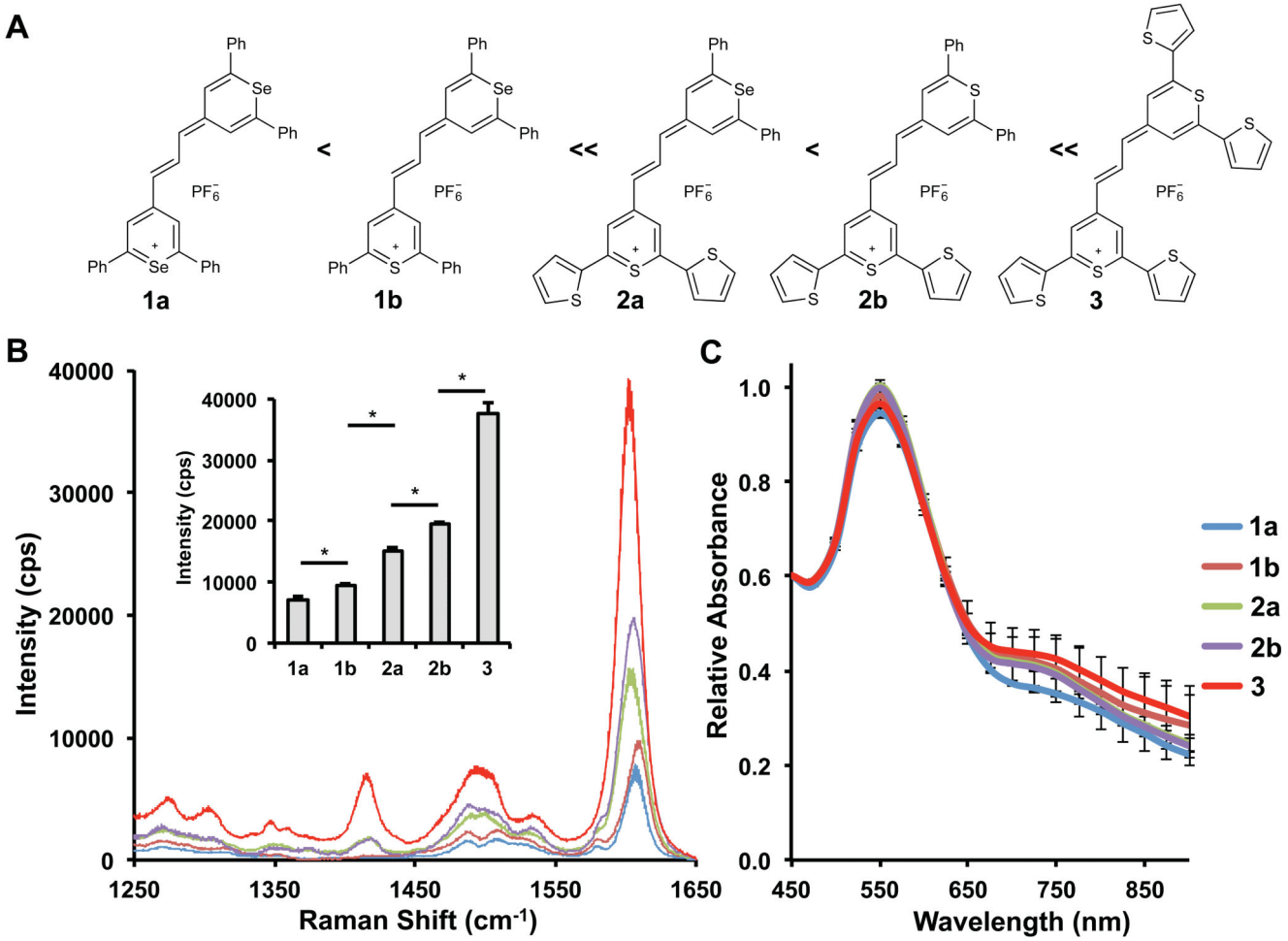

Figure 3. The SERRS-intensity as a function of dye affinity for the gold surface

(**A**) Molecular structures of the adsorbed CP-dyes (**1**–**3**) arranged by increased number of 2-thienyl substituents (Ph, phenyl). (**B**) SERRS spectra of the CP-based SERRS-nanoprobes. The SERRS spectra were baseline corrected to allow proper comparison. (For the non-baseline corrected spectra see Supplementary Figure 3). Inset: intensity of the 1600 cm^{-1} peak (n=3; error bars represent standard deviations, *P<0.05; an unpaired Student's *t*-test was performed). **C**) Colloidal stability of the CP-based SERRS-nanoprobes as determined by LSPR measurements (n=3; error bars represent standard deviations; See also Supplementary Figure 2; Supplementary Table 1).

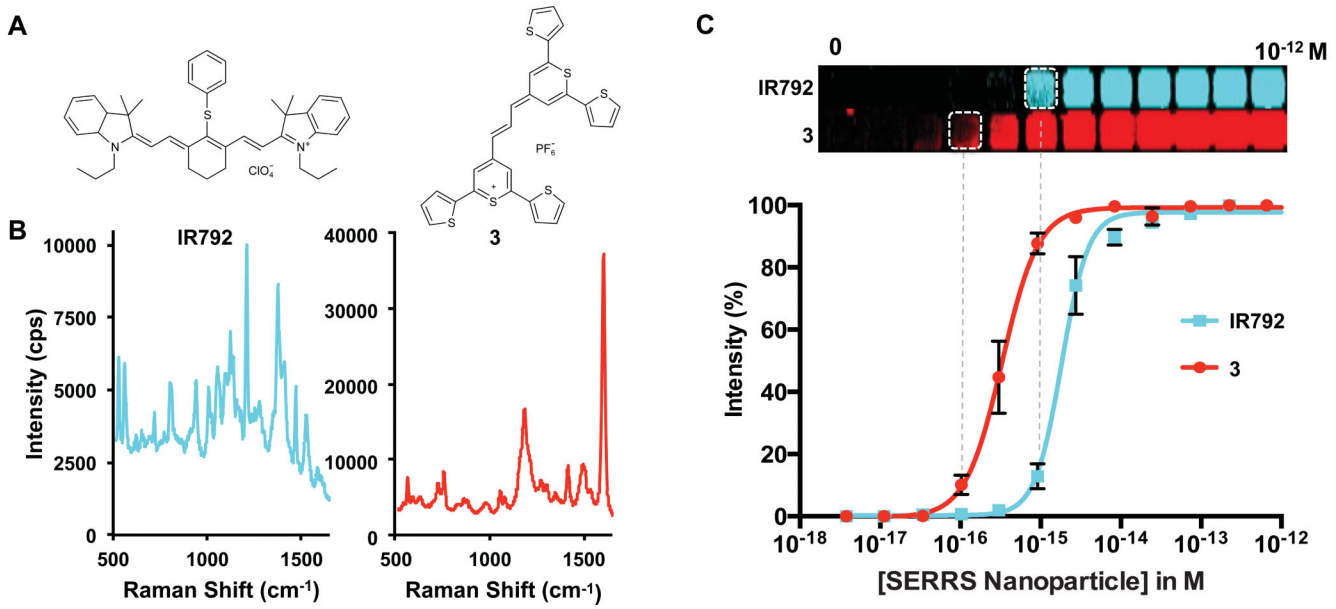

Figure 4. Comparison of the SERRS-signal intensity of the optimized CP-dye 3 versus a widely used resonant dye IR792

(**A**) Structure of the resonant dye **IR792** and chalcogenopyrylium dye **3**. (**B**) SERRS intensity of an equimolar amount of an **IR792**-based SERRS-nanoprobe and a **3**-based SERRS-nanoprobe that were synthesized of an equimolar amount of the dyes. (**C**) Limits of detection of the **IR792**- (cyan) and **3**- (red) based SERRS-nanoprobes were performed in triplicate and determined to be 1.0 fM and 100 attomolar, respectively (See also Supplementary Figure 4).

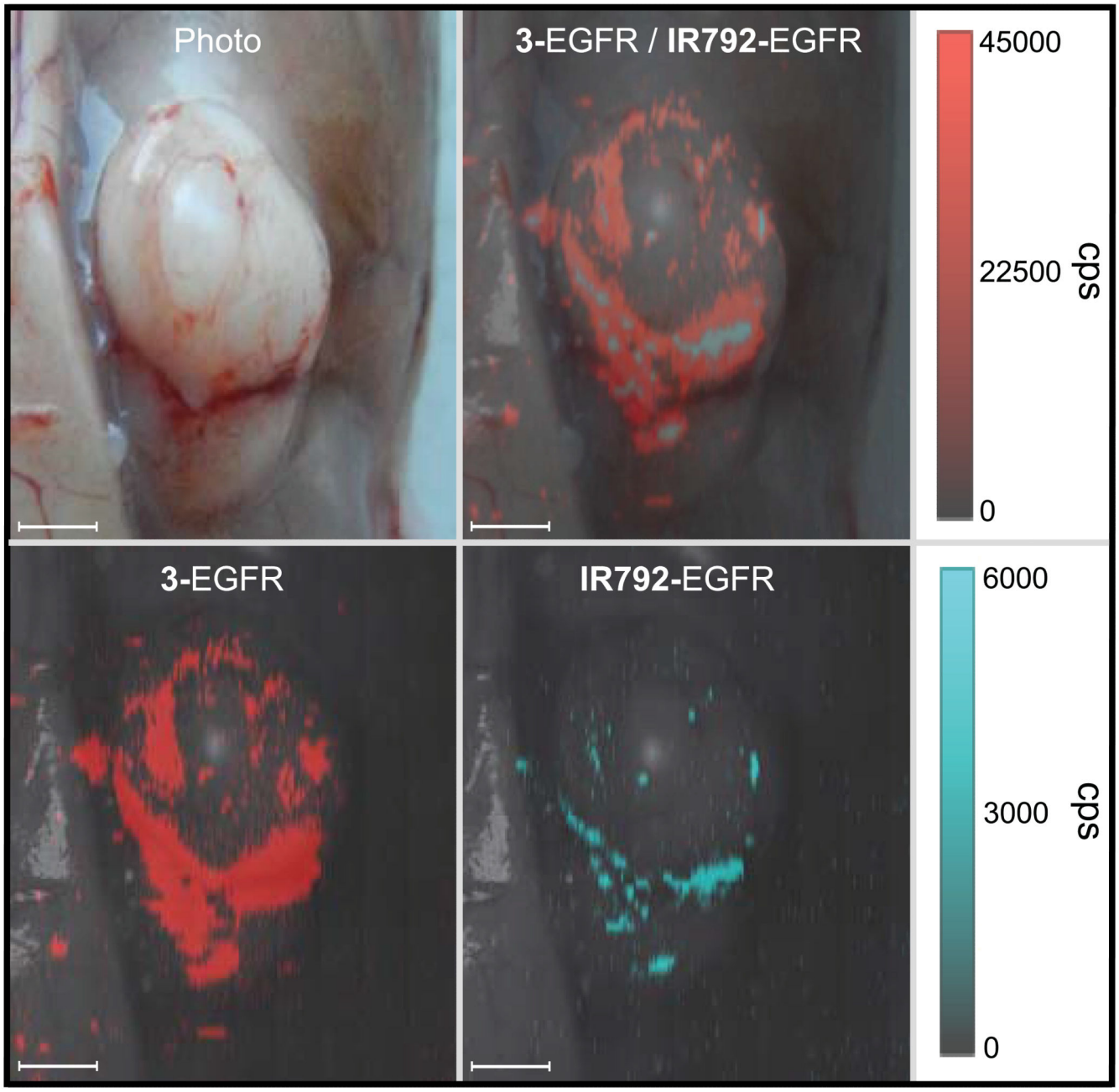

Figure 5. Comparison between EGFR-targeted IR792- or 3-based SERRS-nanoprobes in an A431 tumor xenograft

Female nude mice (n=5) bearing A431 xenograft tumors were injected intravenously via tail vein with an equimolar amount of EGFR-antibody (cetuximab)-conjugated **IR792**- and CP **3**-based SERRS-nanoprobes (15 fmol/g per probe; total injected dose: 30 fmol/g). After 18 hours, the tumors were imaged *in situ* by Raman (10 mW, 1.5 s acquisition time, 5× objective). The chalcogenopyrylium dye **3**-based SERRS-nanoprobe (red) provided ~3× more contrast than the **IR792**-based SERRS-nanoprobe (cyan) (22.442 cps/cm^2 versus 7.313 cps/cm^2, respectively). All scale bars represent 2.0 mm.

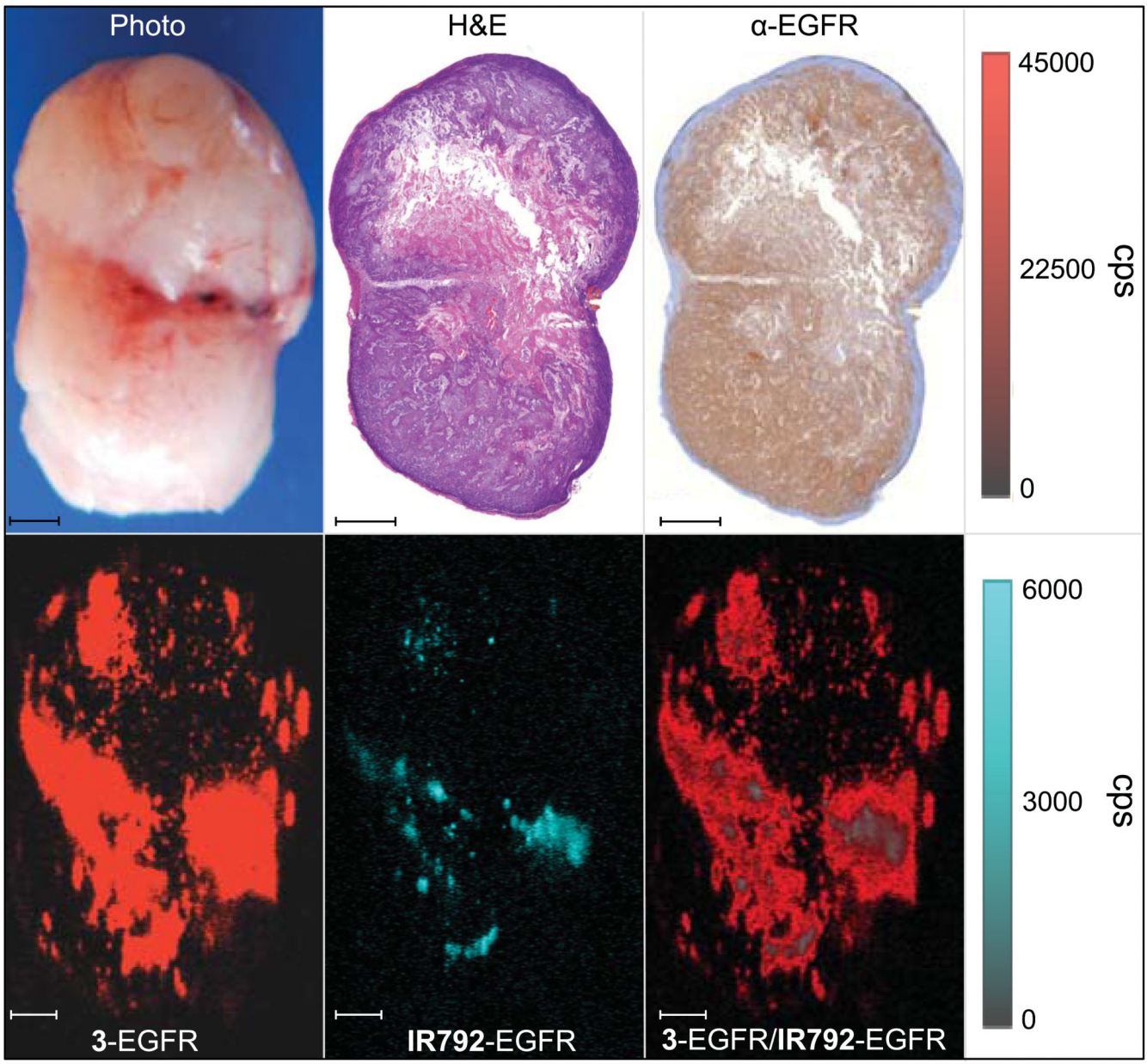

Figure 6. Immunohistochemistry and *ex vivo* Raman imaging of the A431 tumor

The excised tumor was scanned by Raman imaging (10 mW, 1.5 s acquisition time, 5× objective) and subsequently fixed in 4% paraformaldehyde and processed for H&E staining and anti-EGFR immunohistochemistry. With the exception of a hypointense Raman region in the center of the tumor, the tumor homogenously expressed EGFR and the EGFR-targeted SERRS-nanoprobes had accumulated throughout the tumor. The hypointense Raman area corresponds to a highly necrotic region within the tumor, which explains the lack of SERRS-nanoprobe accumulation and decreased Raman signal. All scale bars represent 1.0 mm.

Table 1

Chalcogenopyrylium dye structural and optical characteristics

Dye	X	Y	λmax (CH_2C_{12})	Log (ε)	Yield (%)
1a	Se	Se	806 nm	5.40	86
1b	S	Se	784 nm	5.30	86
2a	S	Se	810 nm	5.40	87
2b	S	S	789 nm	5.34	88
3	S	S	813 nm	5.45	94